Biomass-derived porous aminated graphitic nanosheets for removal of the pharmaceutical metronidazole

Optimization of physicochemical features and exploration of process mechanisms

Bonyadi, Ziaeddin; Noghani, Farzaneh Akhound; Dehghan, Aliakbar; der Hoek, Jan Peter van; Giannakoudakis, Dimitrios A.; Ghadiri, Seid Kamal; Anastopoulos, Ioannis; Sarkhosh, Maryam; Colmenares, Juan Carlos; Shams, Mahmoud

Important note
To cite this publication, please use the final published version (if applicable).
Please check the document version above.

Biomass-derived porous aminated graphitic nanosheets for removal of the pharmaceutical metronidazole: Optimization of physicochemical features and exploration of process mechanisms

Ziaeddin Bonyadi [a,1], Farzaneh Akhound Noghani [a,1], Aliakbar Dehghan [a],
Jan Peter van der Hoek [b], Dimitrios A. Giannakoudakis [c,*], Seid Kamal Ghadiri [d,*],
Ioannis Anastopoulos [e], Maryam Sarkhosh [a], Juan Carlos Colmenares [c], Mahmoud Shams [a,*]

[a] Social Determinants of Health Research Center, Mashhad University of Medical Sciences, Mashhad, Iran
[b] Department of Water Management, Faculty of Civil Engineering and Geosciences, Delft University of Technology, Delft, the Netherlands
[c] Institute of Physical Chemistry, Polish Academy of Sciences, Kasprzaka 44/52, 01-224, Warsaw, Poland
[d] Department of Environmental Health Engineering, School of Public Health, Shahroud University of Medical Sciences, Shahroud, Iran
[e] Department of Chemistry, University of Cyprus, P.O. Box 20537, CY-1678 Nicosia, Cyprus

GRAPHICAL ABSTRACT

ARTICLE INFO

ABSTRACT

The presence of trace levels of pharmaceutically active compounds (PhACs) in the aquatic environment threatens human health and the environment. Metronidazole (M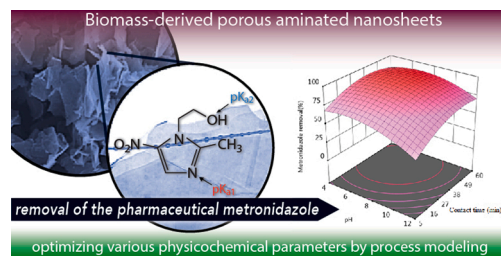NZ) is a soluble PhAC with low biodegradability, a possible human mutant and carcinogen. This study aimed the synthesis, physicochemical characterizations, and employment of porous amine-modified green-graphene (AMGG) for MNZ removal from aqueous solutions. Response-surface methodology (RSM) based on Box-Benken design (BBD) was used to assess the MNZ adsorption efficiency of AMGG as a function of pH (4–12), contact time (5–60 min), AMGG dose (0.1–1 g/L) and MNZ concentration (10–100 mg/L). From the model optimization, the highest MNZ removal was predicted at a pH of 5.9, a contact time of 27 min, an AMGG dose of 0.86 g /L, and an MNZ concentration of 100 mg /L. The experimental data were in agreement with the pseudo-second order kinetic model and the Langmuir isotherm model. The maximum adsorption capacity of AMGG for MNZ was 416.7 mg/g. The MNZ concentration at equilibrium increased about 4.8 mg/L when the solution temperature increased by 20 oC (from 30 to 50 °C), indicative of an exothermic process. AMGG showed an efficiency decrement from 84 % to 57 %, after five

* Corresponding authors.
 E-mail addresses: dagchem@gmail.com (D.A. Giannakoudakis), kamalgh2005@gmail.com (S.K. Ghadiri), ShamsMH@mums.ac.ir (M. Shams).
[1] These authors are co-first author with equal contribution.

consecutive saturation-regeneration cycles. Moreover, AMGG showed a removal efficiency of 74 % when it was employed for real hospital wastewater treatment.

1. Introduction

The substantial influence of antibiotics as essential element in public health care and agriculture as well as livestock farming is well recognized [1–4]. However, the presence of even trace levels of pharmaceutically active compounds (PhACs) and other organic micropollutants in wastewater threatens the environment [5–7]. Most of PhACs are refractory to biological degradation and accumulate in water and soil, where they provoke the development of antibiotic resistance genes and induction of chronic toxicity to aquatic life [8].

A specific PhAC, Metronidazole (MNZ), that belongs to the nitro-imidazole family, is widely used as antibacterial and anti-inflammatory antibiotic [9]. This antibiotic is utilized for treatment of infectious human diseases and also as efficient anti-parasitic agent for chicken and fish cultivation [10]. With a ring-like structure, MNZ is known as a potential human carcinogen and mutant with detrimental effects on white blood cells [11]. Therefore, it is necessary to remove MNZ from polluted aquatic matrixes by effective methods.

The removal of antibiotics from aquatic solutions via conventional methods is often difficult due to their low degradability and high solubility [12]. Various techniques, including advanced oxidation processes [13], adsorption [14,15], biological methods [16], and ultraviolet light degradation [17], have been used to remove antibiotics from aquatic solutions. Each of these methods has advantages and disadvantages. For instance, the environmental benign biological methods need a long treatment time and have very low antibiotic removal efficiencies ranging from 10 to 20 % [18]. The use of methods such as chlorination, nanofiltration, and oxidation have received less attention because of their high costs and low efficiency [19]. Adsorption is a promising option that is widely accepted as benign, economic and easy applicable technique [20]. Although, further studies are required in order to develop new, effective, and cost-effective adsorbent materials to make adsorption more practical for a real-life application.

Graphene is a novel two-dimensional carbon nanomaterial and a fundamental building block for bucky balls, graphite, and carbon nanotubes [21]. This material attracted scientific interest in recent years due to the potential to be utilized for a wide range of applications, with its functionalization/modification to open new routes in materials design potentials [22]. Graphite oxide (GO) which is prepared through the oxidation of graphite [23–25] is proposed as a promising adsorbent with high adsorption capacity for rapid separation of pollutants from water [26,27]. Having epoxy, hydroxyl, and carboxyl groups [28,29], GO is a hydrophilic material and a potential candidate for purification of aqueous environments [30]. To date, GO and GO nanocomposites received tremendous attention for their adsorptive potential for ammonia [31], formaldehyde [22], mercury [32], copper [33] and aromatic compounds [27].

The use of agricultural biomass/waste as precursor for the synthesis of novel adsorbent is among the most prosperous strategies, aligned with the green chemistry and sustainability targets [34]. Although various classes of materials can be derived by the treatment of biomass, such as biochar or carbons, a special focus was given recently on graphene-based materials. It was presented previously that graphitic-based material obtained from corn stover showed an elevated remediation efficiency against antibiotics like tetracycline and ciprofloxacin [14,35,36]. Wheat straw is an abundantly available agricultural biomass/waste, hence the research attention on wheat straw biomass derived adsorbents is elevated the last years [37–39]. Additionally, surface chemistry modification/functionalization of the graphene-based materials can have beneficial effects on the adsorptive capability.

To the best of our knowledge, there is no previous published work on

MNZ removal by amine-modified green-graphene. In the current study, a biomass derived material consisting predominately from GO nano-sheets was prepared through the thermal conversion of wheat straw followed by post modification to form amine-modified green-graphene (AMGG). After characterization of the material, AMGG was used as adsorbent in a series of batch mode experiments to treat in-lab prepared solutions containing MNZ in various concentrations and under a wide range of conditions. The role of independent conditions/variables i.e. pH, contact time, adsorbent dose, and initial MNZ concentration on adsorption efficiency was elucidated by performing the experiments modeling according to Box-Behnken design. Also, the model derived from the Box-Behnken design was used to determine the conditions leading to the highest MNZ removal efficiency. The study covered also the removal of MZN from real hospital wastewater, and the effect of consecutive saturation-regeneration cycles of AMGG on the adsorption capacity.

2. Materials and methods

2.1. Chemicals

All chemicals used in this study were obtained from Merck company, Germany. The properties of metronidazole (MNZ) are shown in Table 1. In all cases, de-ionized water was used.
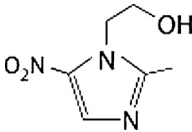
2.2. Green-Graphene nanosheet (gGrNShts) synthesis

gGrNShts was synthesized via thermochemical process. For this purpose, raw wheat straw was first washed thoroughly with tap water and then deionized water to remove dust and other impurities. The solid phases were then dispersed in ethanol (50 %) and sonicated at 30 kHz for 1 h. Subsequently, the clean wheat straw was separated from the mixture by filtration and dried overnight. Next, the wheat straw was thermally treated at 300 °C for 30 min in an oxygen-free environment to yield derived wheat black carbon (WDBC). WDBC was finally crushed and sieved to the size of < 149 μm (100 mesh). To transform WDBC into gGrNShts, 5 g WDBC and 50 g KOH was added to 200 mL de-ionized water and stirred for 24 h. After filtration of the suspension, the solids were thoroughly washed with de-ionized water, dried, crashed and sieved to the size of <149 μm. The product was further activated at 790 °C in an electric furnace with a temperature ramp of 25 °C/min under nitrogen gas flow (0.5 L/min) for 2 h.

2.3. Modification of gGrNShts by grafting amine groups method

Crosslinking of the gGrNShts with epichlorohydrin was performed based on the following synthetic protocol. 20 mL aliquot of epichlorohydrin (99.9 % purity) was added to a solution consisting of 36 mL *N,N*-

Table 1
Details for the studied pharmaceutical, metronidazole (MNZ) [12,40–42].

Property	
Molecular formula	$C_6H_9N_3O_3$
Molecular weight (g/mol)	320
Molecular structure	
pK_{a1}	2.38
pK_{a2}	14.48

dimethylformamide (DMF) and 36 mL triethylamine and then mixed at 80 °C for 2 h in a 500 mL Erlenmeyer. Finally, 30 g gGrNShts was suspended in 90 mL of the solution described above in a 250 mL three-neck round bottom flask. Then 20 mL pyridine (as the catalyst) was added to the mixture and stirred for 2 h at 60 °C. For purification, the resulting mixture was filtered and washed firstly with 500 mL NaOH (0.1 M) and then with 500 mL HCl (0.1 M) and, as the final step, was extensively washed with de-ionized water. Afterwards, the product was dried in a vacuum drier at a temperature of 50 °C for 24 h and sieved to the size of <149 μm. The final obtained material is referred to as AMGG (amine-modified green-graphene).

2.4. Characterization of the adsorbent

XRD analysis was performed by X-ray diffraction (XRD; model: XD-5A) using Cu beam ($\lambda = 1.541$ Å) to identify the potential presence of minerals and to analyze WDBC and AMGG characteristics. Raman was used to identify the molecular structure of compounds using Almega Thermo Nicolet Dispersive Raman Spectrometer equipped with a 785 nm laser source. In addition, Fourier Transform Infrared Spectrometer (EQUINOX 55, Bruker, Germany) in the 399–3998 (cm^{-1}) spectral range was applied to identify the functional groups on the adsorbent surface. The Zeiss-EM10C transmission electron microscope (TEM) at 100 kV was used to determine the morphology of AMGG [43].

2.5. Experimental design for adsorption experiments and adsorption modeling

2.5.1. Adsorption experiments for removal efficiency determination

WDBC, gGrNShts, and AMGG were tested to determine how the adsorption efficiency increased by modifications carried out on virgin wheat straw. This primary evaluation was accomplished by adding 0.5 g/L adsorbent material (WDBC, gGrNShts, and AMGG) to deionized water containing 50 mg/L MNZ at natural pH (5.4), followed by mixing for 30 min. The adsorbent with the highest adsorption efficiency (AMGG) then was used for a full experimental study as described in the following.

100 mL of a MNZ solution was prepared using deionized water with MNZ concentration of 10−100 mg/L, an AMGG dose of 0.1−1 g/L, and a pH of 4–12. The contact time ranged from 5 to 60 min. The samples were mixed at a fixed speed of 250 rpm at room temperature (26 ± 2 °C). When the contact time was completed, a sample of 10 mL was picked up from each Erlenmeyer flask and centrifuged at 4000 rpm for 10 min to separate nanoparticles. Finally, the absorbance of the supernatant and the control sample (the sample without adsorbent) was read using a spectrophotometer at the maximum wavelength (320 ± 7 nm). All the experiments were performed in triplicates with the average values to be presented (the range of error deviation was less than ±6 %)

The MNZ removal efficiency was calculated using the following equation:

$$\text{Removal efficiency } (\%) = \frac{C_0 - C}{C_0} \times 100 \tag{1}$$

Where C_0 is the MNZ concentration in the control sample (mg/L) and C is the MNZ concentration in the treated solution after a given time (mg/L).

The amount of MNZ adsorbed per unit AMGG was determined using the following equation:

$$q_e = \frac{(C_0 - C_e)}{m} \times V \tag{2}$$

Where C_e is the equilibrium concentration of MNZ (mg/L), m is mass of the AMGG adsorbent (g), and V is the volume of the used solution (L).

2.5.2. Modeling of the MNZ removal efficiency

In this study, design expert software based on response surface methodology (RSM), the model of Box-Behnken (BBD), was used to evaluate the effect of independent variables on MNZ removal efficiency [35,44]. Independent variables included pH (A), contact time (B), adsorbent dose (C) and initial antibiotic concentration (D). The different values of the variables are presented in Table 2. The total of experimental runs was 29. The model used in RSM was quadratic which is presented below:

$$Y = \beta 0 + \sum_{i=1}^{k} \beta_i x_i + \sum_{i=1}^{k} \beta_{ii} x_i^2 + \sum_{1 \leq i \leq j}^{k} \beta_{ij} x_i x_j \tag{3}$$

Where Y is the predicted response, β_0 the constant coefficient, β_i the regression coefficients for linear effects, β_{ii} the quadratic coefficients, x_i the interaction coefficients, and x_j the coded values of the parameters. The fit of the model was evaluated by R^2, adjusted R^2, predicted R^2, and adequacy precision [45].

2.6. Adsorption kinetics and adsorption isotherm studies

The experiments to determine the adsorption kinetics were carried out with an AMGG dose of 0.86 g/L, a MNZ concentration of 50–200 mg/L, a pH of 5.9, and a contact time of 10−60 min. The kinetics of MNZ adsorption onto AMGG was studied using the well-known pseudo-first-order, pseudo-second-order and intra-particle diffusion models [46]. The pseudo-first-order model is displayed as Eq. 4:

$$\ln(q_e - q_t) = \ln q_e - k_1 \times t \tag{4}$$

Where k_1 (1/min) is the pseudo-first-order kinetic constant, q_e (mg/g), and q_t (mg/g) are MNZ adsorption capacity of AMGG at equilibrium state, and the MNZ adsorption capacity of AMGG at time t, respectively. The pseudo-second-order model is expressed in Eq. 5:

$$t/q_t = {}^1/{k_2 q_e^2} + {}^1/{q_e} t \tag{5}$$

Where k_2 (g/mg.min) is the rate constant of pseudo-second-order model and q_e and q_t are as described above. The linear form of intra-particle diffusion model is given in Eq. 6:

$$q t = k_p.t^{0.5} + c \tag{6}$$

where k_p and t are intra-particle diffusion rate constant and contact time, respectively, and c is a constant value related to boundary layer [47].

The adsorption isotherms have been surveyed under the following conditions: an adsorbent dose of 0.1−1 g/L, a MNZ concentration of 100 mg/L, a pH of 5.9, and a contact time of 27 min. All the experiments were performed at room temperature (26 ± 2 °C). In this work, the adsorption isotherms were studied using Langmuir, Freundlich, Temkin, and Dubinin-Radeskovich equations. The Langmuir isotherm is described in the following equation:

$$\frac{C_e}{q_e} = \frac{1}{q_m} C_e + \frac{1}{K_L q_m} \tag{7}$$

where q_m (mg/g) and k_L (L/mg) are the maximum sorption capacity and

Table 2
Range and levels of independent variables used for BBD modeling.

Factor		Variable value		
	Code	−1	0	+1
pH	A	4	8	12
Contact time (min)	B	5	32.5	60
AMGG dosage (g/L)	D	0.1	0.55	1
MNZ (mg/L)	C	10	55	100

the Langmuir equilibrium constant, respectively.

The linear form of the Freundlich model is described according to Eq. 8:

$$\ln q_e = \ln K_f + \left(\frac{1}{n}\right)\ln C_e \tag{8}$$

where K_F $((mg/g)*(L/mg)^{1/n})$ and n display the Freundlich constants related to AMGG adsorption capacity and sorption intensity, respectively [48].

Dubinin-Radushkevich isotherm is an empirical adsorption model that is commonly used to describe adsorption mechanisms with Gaussian energy distribution onto heterogeneous surfaces. Dubinin-Radushkevich isotherm is given by the following equation [49]:

$$\ln q_e = \ln q_m - \beta \in^2 \tag{9}$$

where $\in$ =RT ln $(1 + \frac{1}{C_e})$ is the Polanyi potential, β is the Dubinin-Radushkevich constant, R is the gas constant (8.31 J/mol. k) and T is the absolute temperature.

Temkin isotherm considers the impacts of indirect adsorbate/adsorbate interactions on the adsorption process. In this model, it is also presumed that the adsorption heat (ΔH_{ads}) of all molecules in the layer reduces linearly due to the increase of surface coverage. The Temkin isotherm is suitable only for an intermediate ionic solution. The linear form of the Temkin isotherm model can be described as follows [50]:

$$q_e = \frac{RT}{b}\ln K_t + \frac{RT}{b}\ln C_e \tag{10}$$

where R is the universal gas constant, T is the absolute temperature, b is the Temkin constant which is related to the heat of sorption and K_t is the Temkin isotherm constant (L/g) [51,52].

2.7. Effect of temperature

The experiments to determine the effect of temperature on MNZ removal efficiency were carried out in 100 mL reaction solutions with the conditions 0.86 g/L AMGG, pH 5.9, MNZ concentration 100 mg/L, contact time 27 min, and temperature 303−323 K.

2.8. Zero point of charge (pH_{zpc}) determination

For determining pH_{zpc}, the pH of a series of 100 mL solutions containing 0.01 M NaCl was adjusted between 2–12. Then, 1 g/L AMGG was added into the reaction solutions and agitated by a magnetic mixer at a fixed speed of 250 rpm for 24 h and filtered over a Whatman paper 42. Finally, the difference between the initial and final pH values or "$\Delta pH = pH_i - pH_f$" was plotted versus pHi [53].

2.9. Regeneration study

In order to choose the appropriate eluting solution, the saturated adsorbent was initially tested for regeneration using acidic (pH = 4) and alkaline (pH = 10) water solutions. The adsorbent then was subjected to a series of saturation/regeneration cycles by the eluting solution, which showed a better performance (the acidic solution). The efficiency of MNZ removal after regeneration was monitored to determine the reusability of the adsorbent.

2.10. Treatment of real wastewater

To determine the practical use of AMGG, adsorption experiments were also carried out using real wastewater samples containing MNZ and other co-current ions. The samples were picked up from a hospital. The experiments were conducted under the optimal conditions (AMGG dose 0.89 g/L, pH 5.9 contact time 27 min).

3. Results and discussion

3.1. Characterization

3.1.1. X-ray powder diffraction (XRD)

The XRD patterns of wheat derived black carbon (WDBC) and of Green-Graphene nanosheet (gGrNShts) are presented in Fig. 1. The pattern of WDBC revealed several peaks at two theta angles of around 23, 26, 28 and 40°, which can be linked to the presence of minerals. After the thermo-chemical treatment, a broad peak was observed from 20 to 30 2θ, with a maximum at around 2θ = 25°, which can be related to the main index of graphite (2θ = 26°), with an interlayer space of around 3.34 Å [54]. The low intensity and broadness of the reflection can be associated with the nano scaled structure and a high level of exfoliation leading to an amorphous in nature graphene sheets organization in gGrNShts [55,56]. The results are consistent with similar studies of XRD patterns of other materials obtained by analogues synthetic processes suing acricultural biomass as a precursor and typical for reduced graphene oxide [55,57]. Moreover, no peaks related to the presence of minerals as in the case of the precursors were observed, suggesting their removal upon the final stage of treatment.

3.1.2. Raman and FTIR

Based on the RAMAN spectrum, D band appeared at around 1333 cm^{-1}, indicating the amorphous carbon phase at the edge plane of graphene sheets or/and in between the graphitic phase [58]. The G band characteristic for the sheets of graphene appeared around 1585 cm^{-1}. According to the result of Fig. 2, the thermo-chemical treatment was significantly affected the D band of the gGrNShts spectrum. The I_G/I_D ratio increased upon modification suggesting an increase of the graphitic phase to amorphous ratio. Thus, the synthesized gGrNShts is characterized with a higher ratio of clean edges and less amorphous carbon phase.

Fig. 3 displays the FTIR spectra for WDBC, gGrNShts, and AMGG. For gGrNShts and AMGG, a broad band is observed at 3400 cm^{-1} which can be ascribed to the presence of the OH groups on the adsorbent surface. The bands observed at 1080 cm^{-1} and 1339 cm^{-1} may be attributed to vibrations of C—O and CO—H groups in the structure of gGrNShts, respectively [43]. The band in the range of 1367 cm^{-1} (that appeared in the FTIR spectrum of AMGG) is related to the stretching vibrations caused by C—N bonding. The bands of the oxygen-containing functional groups and the alkenyl and hydroxyl groups (with wavenumbers of 1635 and 3431 cm^{-1}, respectively) remained on the AMGG surface.

3.1.3. Transmission electron microscopy (TEM)

The structure and morphology of gGrNShts was investigated by TEM analysis. Based on the TEM image (Fig. 4), gGrNShts has a thin, flattened and few-layers structure.
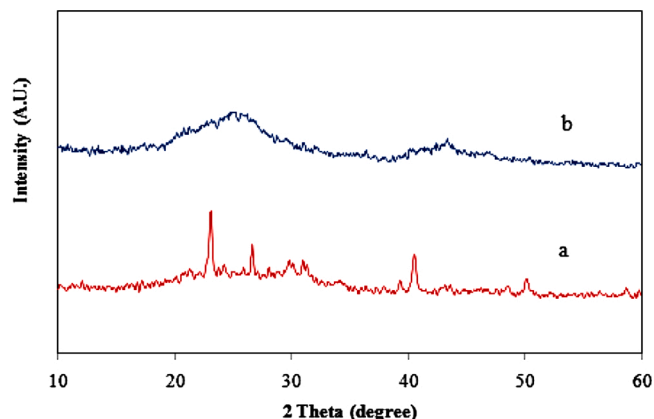

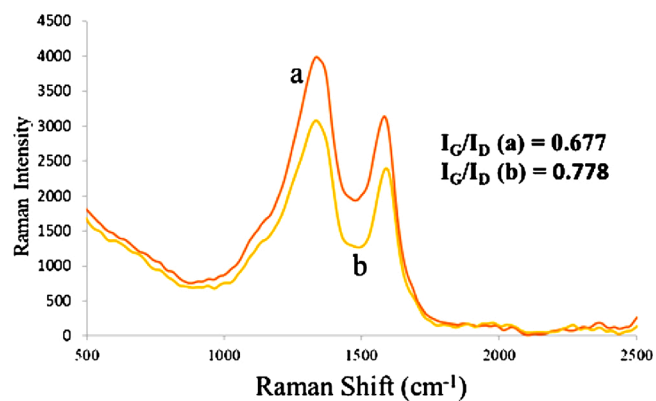**Fig. 1.** The XRD pattern of WDBC (a) and gGrNShts (b).

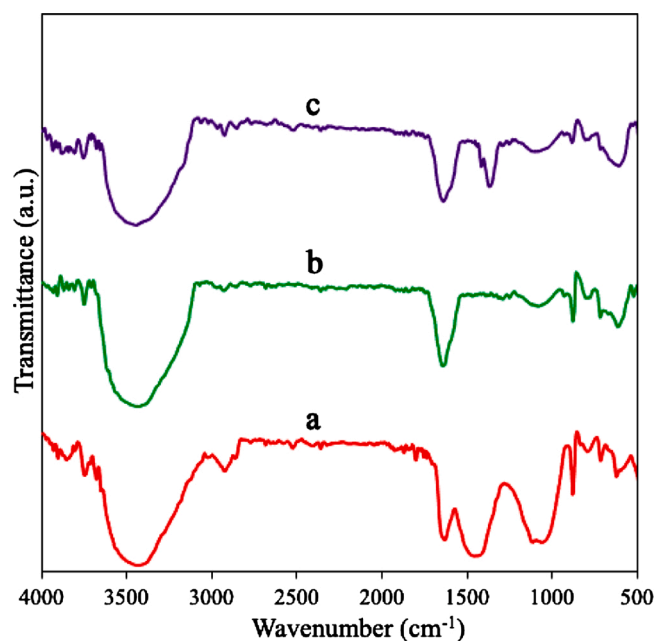**Fig. 2.** RAMAN spectra of WDBC (a) and gGrNShts (b).

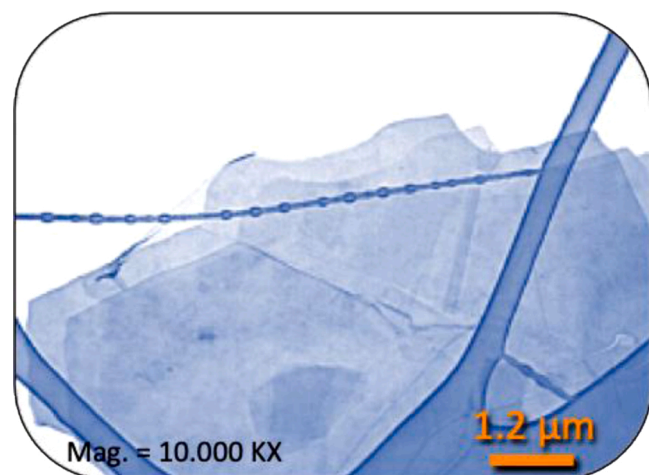**Fig. 3.** FTIR spectra of WDBC (a), gGrNShts (b) and AMGG (c).

Fig. 4. TEM image of the gGrNShts (the initial images can be found at the Supplementary Information).

3.1.4. Scanning electron microscope (SEM)

Fig. 5 collects the SEM images of WDBC combusted at 300 °C, gGrNShts and AMGG. The AMGG nanosheets are clearly visible. The uniform structure of the graphitic nanosheets indicates that due to the proper final elution of the product and its optimum synthesis, no salt crystals and other impurities are present [59]. The SEM images show that the structure of AMGG is more uniform than gGrNShts. This is due to the existence of amino groups in the structure of AMGG [60].

3.1.5. Brunauer-Emmett-Teller (BET)

The BET specific surface area (S_{BET}) and porosity information derived from the analysis of the nitrogen physisorption tests of the products are shown in Table 3. The S_{BET} of gGrNShts was higher than other adsorbents such as nanopores of doum palm shell derived carbon prepared by NaOH activation (226 m^2/g) [61], hydrothermally reduced graphene oxide (364 m^2/g) [62], Fe$_2$O$_3$/RGO composite (32 m^2/g) [63], nitrogen-doped RGO (146.0 m^2/g) [64], hydrothermally modified RGO (~181 m^2/g) [65] and is almost similar to commercial reduced graphene oxide of Sigma-Aldrich with S_{BET} of around 450 m^2/g.

3.2. Preliminary adsorption study

WDBC, gGrNShts, and AMGG were synthesized and tested to determine how MNZ adsorptive properties improved by wheat straw modification. The best material among the synthesized adsorbents then was chosen for the following optimization experiments. Fig. 6 shows that AMGG had the highest removal efficiency in the preliminary study, reaching 84 % removal efficiency, a value more than 3 folds higher than
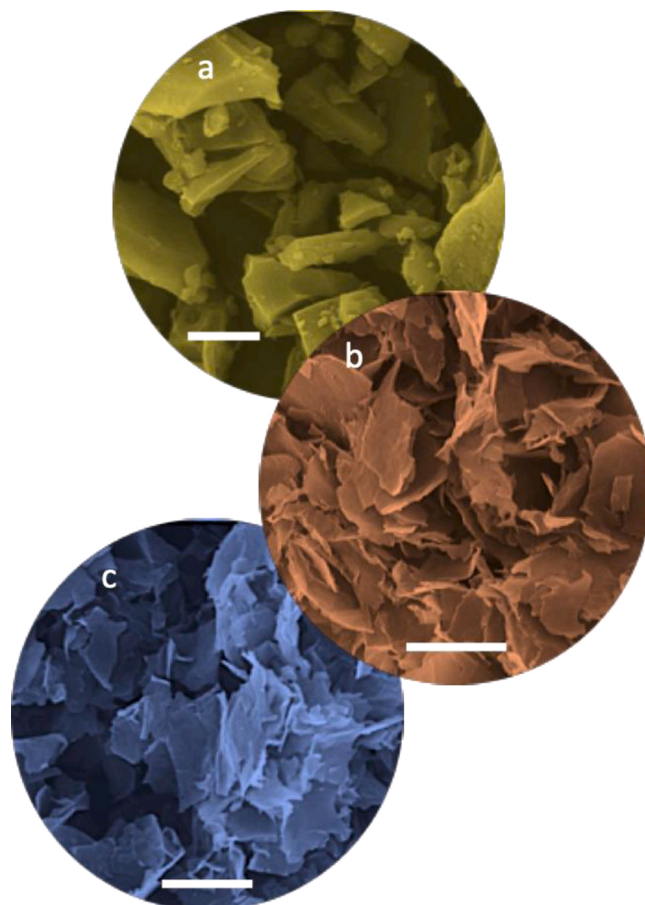

Fig. 5. SEM image of the WDBC (a), gGrNShts, and AMGG (c); scale bars represent 10 μm while the original images can be found at the Supplementary Information.

Table 3
The BET specific surface area and porosity information of the products.

S_{BET} (m^2/g)	Total pore volume (cm^3/g)	Mean pore diameter (nm)	Material
7	0.028	15.9	Raw wheat straw (< 149 μm)
50	0.094	5.1	WDBC
423	0.305	2.6	gGrNShts
389	0.273	2.8	AMGG
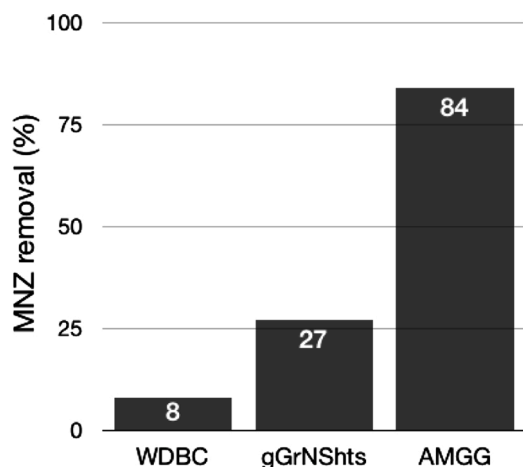
Fig. 6. Comparison of MNZ removal efficiency for WDBC, gGrNShts and AMGG (adsorbent dosage: 0.5 g/L, contact time: 30 min, initial MNZ concentration: 50 mg/L, solution/suspension pH: 5.4).

that of gGrNShts.

3.3. Analysis of the RSM model for MNZ removal

By the utilization of AMGG to a series of solutions containing MNZ according to the design, experimental data were collected. Table S1 in the supplementary information (SI) shows the observed values of MNZ removal efficiency (%). According to the findings in Table S1, the minimum and maximum observed removal efficiencies were 16 % and 92 %, respectively.

The experimental results were statistically analyzed for linear, 2Fl, quadratic and cubic models to select the model that best describes the data. The results of comparative model regression are collected in Table S2 (SI). In this work, the quadratic model was the best fitted model for the experimental data. Table S3 (SI) presents the analysis of variance (ANOVA) for the response surface quadratic model. Overall, a P-value <0.05 indicated that the model was significant. From Table S3, R^2, adjusted R^2, predicted R^2, and adequacy precision were 0.97, 0.95, 0.87, and 20.82, respectively.

For each model term in Table S3, a P-value lower than 0.05 shows that the term has a statistically and significant effect on MNZ adsorption. Moreover, for a statistically acceptable model, the Lack of Fit (LOF) F-value should be higher than 0.05. The LOF F-value for the present work was found to be 0.07. It is recommended that the difference between adjusted R^2 and predicted R^2 should be lower than 0.2, which is the case for the model [66]. The adequacy precision term measures the signal to noise ratio. This parameter was 20.8 which is quite beyond the minimum desirable value of 4. The adequacy of the model to give a good prediction for MNZ removal is clearly illustrated in Table S1 (SI) and Fig. 7, which shows the experimental removal versus the predicted removal.

The quadratic model for MNZ removal by AMGG is presented in Eq. 11:
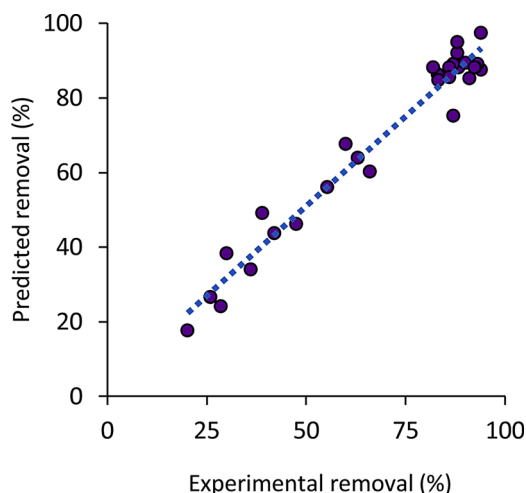
Fig. 7. Experimental (dots) vs. predicted (dashed line) MNZ removal by AMGG.

$$MNZ\ Removal\ (\%) = 90.10 - 8.9\ A + 10.13\ B + 22.35\ C - 13.24\ D + 2.78\ AB - 7.86\ AC - 4.6\ AD + 10.20\ BC + 9.58\ BD + 10.33\ CD - 11.64\ A^2 - 11.89\ B^2 - 25.29\ C^2 + 2.81\ D^2 \tag{11}$$

Where, A = pH, B = contact time, C = AMGG dose and D = MNZ concentration. In the above equation, each model term has a positive or negative sign which is indicative of its increasing / reducing effect on the response, i.e. the MNZ removal. The MNZ removal is proportionally increased by contact time (B) and AMGG dose (C) and proportionally decreased by pH (A) and MNZ concentration (D). From Eq. 11, with the highest coefficient of +22.35, AMGG dose (C) had the greatest impact on the removal of MNZ.

3.4. The effect of process variables on MNZ removal by AMGG

Based on the RSM model, the effect of process variables (pH, contact time, adsorbent dose and initial antibiotic concentration) on MNZ removal by AMGG was evaluated. The pH_{zpc} of AMGG was found to be about 8.3. Thus, its surface would be positive, neutral and negative at a pH lower than 8.3, at a pH of 8.3 and at a pH above 8.3, respectively. Metronidazole is a weak base with $pKa_1 = 2.38$ and $pKa_2 = 14.48$ [12, 42]. At pH value below 4, MNZ is in its protonated form ($MNZ-H^+$), since the imidazoline nitrogen is positively charged. Between pH 4 and ~12, MNZ is neutral (MNZ), since imidazoline nitrogen is de-protonated. Beyond pH 12, the hydroxyl group is ionized as so the MNZ is negatively charged (MNZ^-). The correlation of the charges of MNZ and the surface of AMGG are summarized in Fig. 8. Since the electrostatic interactions are of repulsive nature at the entire tested range of pH, the observed adsorption efficiency of AMGG can be linked to different interactions such as π-π interactions/stacking, Van der Waals forces, and hydrogen bonds.

Fig. 9(a–c) displays the effect of pH, AMGG dose, MNZ concentration, and contact time on MNZ removal. In most sorption systems the pH is a critical factor that affects the adsorbent surface charge and pollutant ionic state. Fig. 9a shows that the removal efficiency was highest at a pH ranging from 5 to 8. At a pH above 8 and under strong acidic conditions, the MNZ removal was decreased. MNZ, on the other hand, is protonated at a pH below 4. Therefore, the MNZ removal decreased due to the electrostatic repulsion between the adsorbent surface and the $MNZ-H^+$ [67,68]. At a pH above 8, the negative charge of the adsorbent surface and MNZ^- molecules led to a decreasing removal efficiency again due to the repulsive electrostatic interactions. Therefore, the highest MNZ removal was expected at a pH around neutral or close to the point of zero charge of the adsorbent.

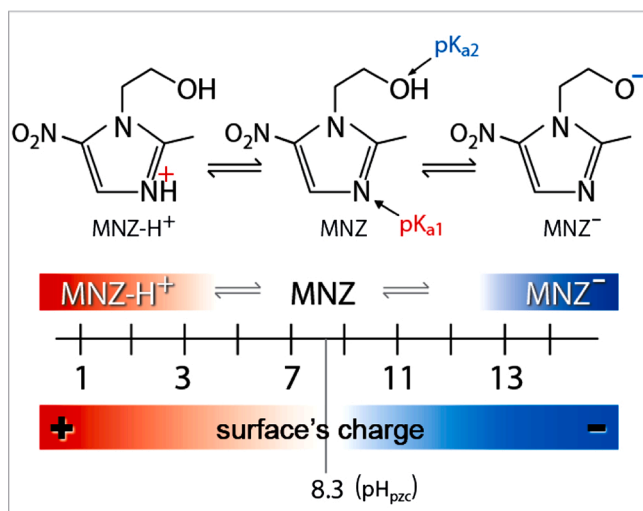The impact of AMGG dose on MNZ removal is displayed in Fig. 9b.

Fig. 8. The charge dependence of the MNZ and adsorbent with solution pH.

With increasing AMGG dosage, the MNZ removal increased initially (at an AMGG dose of 0.1−0.86 g/L) and then decreased slowly (at an AMGG dose of 0.86−1 g/L). The increase in MNZ removal at an adsorbent dose up to 0.86 g/L is related to an increasing available sorption surface for MNZ. The lower mobility of the AMGG particles, on the other hand, is probably responsible for decreasing MNZ removal when the adsorbent dose was adjusted to above 0.86 g/L [69,70].

Fig. 9b shows that the contact time directly affects the MNZ removal. Interestingly, high removal already occurred after a short contact time and highest MNZ removal was at 30 min contact time. The slope of the MNZ removal gradually decreased above 30 min contact time.

According to Fig. 9c, there is a relationship between the initial MNZ concentration and its removal efficiency. A higher initial concentration resulted in a lower removal efficiency. The saturation of the sorbent sites of AMGG at high MNZ concentrations is the reason for this behavior. At low MNZ concentrations, the ratio of the active AMGG sites for adsorption to the initial number of MNZ molecules is high, and as a result, the removal will be independent of the concentration at low initial concentrations [67].

3.5. Optimum operational conditions

The present work aimed to optimize the operational condition to reach the highest removal. The optimization was performed by using Eq. 11 to maximize the response. The range of independent variables were considered in the coded levels of ± 1, as used for BBD design. From the quadratic model optimization, the highest MNZ removal (theoretically 100 %) was obtained at a pH of 5.9, a contact time of 27 min, an adsorbent dose of 0.86 g /L, and a MNZ concentration of 100 mg /L. This optimum situation was experimentally tested and the average MNZ removal in three repeated tests was found to be 97.4 %, which is close to that predicted by the model.

3.6. MNZ adsorption kinetics and isotherm studies

Kinetics are an important part of any sorption study that simulates the rate of solute uptake from the solute-solution interface [71]. Kinetic models provide valuable information about the economy of adsorption by determining the rate constants and hence the contact time and volume of an adsorption unit. The models also could reveal the rate control step in the sorption process [72]. In this study, the common kinetic models, including pseudo-first-order, pseudo-second-order and intraparticle diffusion kinetic models [73,74] were used to elucidate the reaction rate coefficients. Table 7 shows the kinetic and isotherm
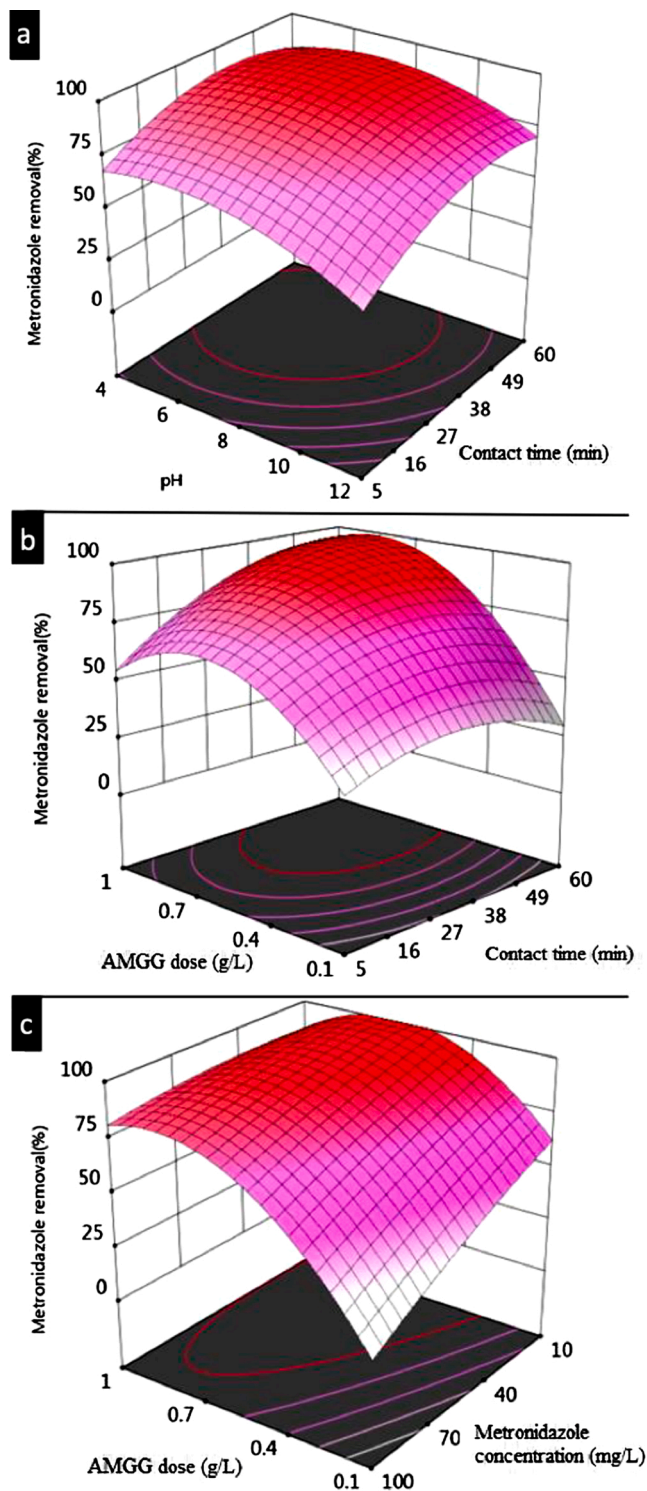
Fig. 9. Response surface plot of the effects of pH vs. reaction time (a), AMGG dose vs. reaction time (b) and AMGG dose vs. MNZ concentration (c).

parameters fitted for MNZ removal by AMGG. Based on the findings, R^2 values for pseudo-first-order, pseudo-second order and intraparticle diffusion kinetics were 0.912, 0.990, and 0.960, respectively, suggesting that the pseudo second-order kinetic model resulted in the best fit. Similar results have been reported by other researchers for MNZ sorption onto carbon materials [67].

The adsorption isotherm, which describes the relation of the solute equilibrium concentration and the solute mass loaded on adsorbent

[75], is also an essential element of sorption studies. The isotherm models are beneficial to understand the surface characteristics, affinity and capacity of the adsorbent toward the adsorbate [76]. The Freundlich [77], Langmuir [42], Temkin [43] and Dubinin–Radushkevich [78] isotherm models were applied.

From Table 4, the Langmuir isotherm was the best fitted model ($R^2 = 0.96$).

The q_{max} values obtained by the fitting of Langmuir model provide a useful tool to compare different adsorbents for a specific contaminant. As shown in Table 5, the highest monolayer adsorption capacity of AMGG obtained in this study is higher than various adsorbents presented in the table.

3.7. Effect of solution temperature

As solution temperature is an important variable in sorption processes, the effect of temperature in the range of 303–323 K was studied. The MNZ concentration at equilibrium increased by temperature in the studied range from 49 to about 53.8 mg/L. This observation suggests the MNZ removal by AMGG is exothermic in nature.

3.8. Reusability of the AMGG sorbent

A potential reusability is an important environmental and economic aspect for an adsorbent. To study the reusability of AMGG, a preliminary test was conducted to elucidate whether alkaline (pH 10) or acid (pH 4) aqueous solute has a better performance in desorbing MNZ molecules from used AMGG. For this, MNZ saturated AMGG was agitated with extracting solutions for 24 h and the adsorbent was then separated and used for an additional sorption cycle. Fig. 10a shows that the MNZ removal efficiency for AMGG, regenerated with acidic water solute, was 77 % compared to 71 % for alkaline solution. Fig. 10b shows that MNZ removal by AMGG in five consecutive adsorption/desorption (acidic regeneration) cycles decreased from 84 % to 57 %. This pattern indicates that the AMGG could be used successfully in consecutive cycles with an acceptable efficiency loss. The reasons behind the declining adsorptive

Table 5
Highest reported capacity for different adsorbents against MNZ.

Reference	Highest reported capacity (mg/g)	Adsorbent
[79]	63.84	PPY-PANi copolymer
[80]	5.05	The polypyrrole (PPy)
[81]	332	Fe_3O_4/Cellulose Nanocomposite
[82]	49.03–97.06	Fe_3O_4-chitosan nano-adsorbent
[83]	190	Graphene oxide (GO)
[84]	200.2	UiO-66
[84]	265.5	UiO-66-NH2
[12]	147	$FeNi_3/SiO_2/CuS$ nanocomposite
[85]	84.55	MgO nanoparticles
[86]	36.89	$CoFe_2O_4$ /Activated Carbon@Chitosan
[87]	110–166	Carbon xerogel/graphene hybrids
[88]	180.74	Microwave-assisted K_2CO_3 activated carbon
This study	416.7	AMGG
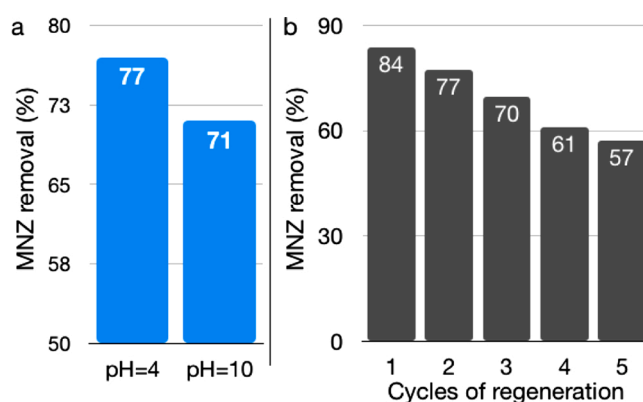
Fig. 10. AMGG reusability; MNZ removal efficiency for AMGG regenerated by alkaline/acid eluting solution (a) and MNZ removal in consecutive adsorption/desorption cycles (b).

efficiency can be various, like blockage of the active adsorption sites, strong/chemical in nature interactions that altered the surface chemistry heterogeneity, or/and not a complete desorption. To study this behavior is a complex aspect outside our research goals at this work. The XRD analysis (Figure S3) of the exposed to MNZ adsorbent (AMGG@MNZ) showed that the amorphous nature was retained and no crystals of MNZ were deposited on the material's surface. The FTIR spectrum of AMGG@MNZ (Figure S4) showed news bands, that can be linked to the MNZ moieties, strongly retained at different in chemical nature adsorption sites/functionalities.

3.9. MNZ removal from real wastewater

Table S4 summarizes the microbiological and physicochemical properties of hospital wastewater, which was treated by AMGG for MNZ removal. The sample was picked up from the effluent of a secondary sedimentation tank after an activated sludge reactor. Due to the negligible concentration of MNZ in the wastewater, MNZ was spiked to a concentration of 100 mg/L. The pH and adsorbent dose were adjusted to 5.9 and 0.89 g/L and the sample was mixed for 27 min. The average MNZ removal in three repeated tests was 74 ± 3.4 %. The lower MNZ removal from real wastewater, compared to MNZ removal from the prepared solutions (97.4 %), is due to the competition between co-current substances, especially organic materials in the mg/L range, and spiked MNZ present in the wastewater. Similar findings have been reported for adsorption of other antibiotics in wastewater by activated carbon and bentonite [89,90].

Table 4
The kinetic and adsorption isotherm parameters fitted for MNZ removal by AMGG.

Kinetic Model	Parameter	MNZ concentration		
		50 mg/L	100 mg/L Value	200 mg/L
Pseudo-first order	$q_{e,cal}$ [mg/g]	11.57	41.2	98.9
	K_1 [1/min]	−0.01	−0.04	0.06
	R^2	0.67	0.89	0.91
Pseudo-second order	$q_{e,cal}$ [mg/g]	55.1	102.3	168.6
	K_2 [g/mg min]	0.02	0.01	0.01
	R^2	1	0.99	0.99
Intra-particle diffusion	K_p [mg/(gmin^{0.5})]	1.05	6.28	8.86
	R^2	0.94	0.89	0.96
Adsorption isotherm model	**Parameter**	**Value**		
Langmuir	q_{max} (mg/g)	416.7		
	K_L (L/mg)	0.014		
	R^2	0.96		
Freundlich	K_F (mg/g)(L/mg)$^{1/n}$	50.8		
	n	3.1		
	R^2	0.9		
Temkin	k_t (L/mg)	1.01		
	B_1	69.5		
	R^2	0.92		
Dubinin–Radushkevich	q_{max} (mg/g)	279.5		
	β	3.65		
	R^2	0.79		

4. Conclusions

In this paper, biomass derived and functionalized green-graphitic material (AMGG) was synthesized by grafting amine groups and applied towards adsorption studies against a hazardous pharmaceutical, metronidazole (MNZ). The adsorbent physicochemical features were surveyed by XRD patterns, FTIR and Raman spectroscopy, TEM and SEM imaging, as well as N_2 adsorption/desorption tests. The specific surface area and total pore volume of AMGG were 389 m^2/g and 0.273 cm^3/g, respectively. From the quadratic model optimization, the highest achievable MNZ removal was occurred at a pH 5.9, a contact time of 27 min, an adsorbent dose of 0.86 g /L, and a MNZ initial concentration of 100 mg /L. These optimum parameters were adapted, leading to an experimentally MNZ removal was found to of 97 %. Langmuir isotherm showed the best fit for MNZ adsorption by AMGG ($R^2 = 0.96$). The kinetics were best described by the pseudo-second-order kinetic model. Moreover, AMGG could be used successfully at least five times after regeneration for MNZ removal. In real hospital wastewater, the MNZ removal efficiency was found to be 74 %. This work reveals that the utilization of abundantly available biomass and biowastes as feedstocks towards the synthesis of novel adsorbents to be applied for environmental remediation process is still an open field of sustainability-oriented research.

CRediT authorship contribution statement

Ziaeddin Bonyadi: Writing - original draft. **FarzanehAkhound Noghani:** Investigation. **Aliakbar Dehghan:** Writing - original draft. **Jan Peter van der Hoek:** Writing - review & editing. **Dimitrios A. Giannakoudakis:** Writing - review & editing, Visualization, Methodology. **Seid Kamal Ghadiri:** Formal analysis, Investigation. **Ioannis Anastopoulos:** Writing - review & editing, Methodology. **Maryam Sarkhosh:** Formal analysis. **Juan Carlos Colmenares:** Writing - review & editing. **Mahmoud Shams:** Conceptualization, Methodology, Formal analysis, Investigation, Writing - original draft, Project administration.

Declaration of Competing Interest

The authors declare that they have no known competing financial interests or personal relationships that could have appeared to influence the work reported in this paper.

Acknowledgement

Appendix A. Supplementary data

Supplementary material related to this article can be found, in the online version, at doi:https://doi.org/10.1016/j.colsurfa.2020.125791.

References

[1] S.B. Zaman, et al., A review on antibiotic resistance: alarm bells are ringing, Cureus 9 (6) (2017).

[2] H. Peng, et al., Two-dimension N-doped nanoporous carbon from KCl thermal exfoliation of Zn-ZIF-L: Efficient adsorption for tetracycline and optimizing of response surface model, J. Hazard. Mater. 402 (2021) 123498.

[3] M. Fu, et al., Ozone-based regeneration of granular zeolites loaded with acetaminophen, Sep. Purif. Technol. (2020) 117616.

[4] C.J. Houtman, et al., Human health risk assessment of the mixture of pharmaceuticals in Dutch drinking water and its sources based on frequent monitoring data, Sci. Total Environ. 496 (2014) 54–62.

[5] T. Rasheed, et al., Environmental threatening concern and efficient removal of pharmaceutically active compounds using metal-organic frameworks as adsorbents, Environ. Res. (2020) 109436.

[6] J. Cao, et al., Peroxymonosulfate activation of magnetic Co nanoparticles relative to an N-doped porous carbon under confinement: boosting stability and performance, Sep. Purif. Technol. 250 (2020) 117237.

[7] Y. Doekhi-Bennani, et al., Simultaneous removal of ammonium ions and sulfamethoxazole by ozone regenerated high silica zeolites, Water Res. 188 (2021) 116472.

[8] S. Afsa, et al., Occurrence of 40 pharmaceutically active compounds in hospital and urban wastewaters and their contribution to Mahdia coastal seawater contamination, Environ. Sci. Pollut. Res. 27 (2) (2020) 1941–1955.

[9] M. Malakootian, N. Olama, A. Nasiri, Photocatalytic degradation of metronidazole from aquatic solution by TiO 2-doped Fe 3+ nano-photocatalyst, Int. J. Environ. Sci. Technol. 16 (8) (2019) 4275–4284.

[10] F. Bahrami Asl, et al., Removal of metronidazole from aqueous solution using ozonation process, J. Mazandaran Univ. Med. Sci. 24 (121) (2015) 131–140.

[11] M. Farzadkia, et al., Photocatalytic degradation of Metronidazole with illuminated TiO 2 nanoparticles, J. Environ. Health Sci. Eng. 13 (1) (2015) 35.

[12] N. Nasseh, et al., Adsorption of metronidazole antibiotic using a new magnetic nanocomposite from simulated wastewater (isotherm, kinetic and thermodynamic studies), Compos. Part B Eng. 159 (2019) 146–156.

[13] X.Z.C.Z.L. Jianming, Comparison of metronidazole degradation by different advanced oxidation processes in low concentration aqueous solutions, Chin. J. Environ. Eng. 3 (2009) 018.

[14] S.K. Ghadiri, et al., Valorization of biomass into amine- functionalized bio graphene for efficient ciprofloxacin adsorption in water-modeling and optimization study, PLoS One 15 (4) (2020) p. e0231045-e0231045.

[15] A. Geczo, et al., Mechanistic insights into acetaminophen removal on cashew nut shell biomass-derived activated carbons, Environ. Sci. Pollut. Res. - Int. (2020).

[16] A. Sadeghi, et al., Ability of the yeast Saccharomyces cerevisiae for biological removal of ciprofloxacin antibiotic in aqueous solution, J. North Khorasan Univ. Med. Sci. 7 (1) (2015) 71–79.

[17] R.F. Dantas, et al., Direct UV photolysis of propranolol and metronidazole in aqueous solution, Chem. Eng. J. 158 (2) (2010) 143–147.

[18] K. Kestioğlu, T. Yonar, N. Azbar, Feasibility of physico-chemical treatment and advanced oxidation processes (AOPs) as a means of pretreatment of olive mill effluent (OME), Process. Biochem. 40 (7) (2005) 2409–2416.

[19] H. Khani, et al., Multi-walled carbon nanotubes-ionic liquid-carbon paste electrode as a super selectivity sensor: application to potentiometric monitoring of mercury ion (II), J. Hazard. Mater. 183 (1–3) (2010) 402–409.

[20] H. Sadegh, G. Ali, Potential Applications of Nanomaterials in Wastewater Treatment: Nanoadsorbents Performance, 2018.

[21] Ce.Ne.R. Rao, et al., Graphene: the new two-dimensional nanomaterial, Angew. Chem. Int. Ed. 48 (42) (2009) 7752–7777.

[22] Y. Matsuo, et al., Removal of formaldehyde from gas phase by silylated graphite oxide containing amino groups, Carbon 46 (8) (2008) 1162–1163.

[23] A.B. Bourlinos, et al., Graphite oxide: chemical reduction to graphite and surface modification with primary aliphatic amines and amino acids, Langmuir 19 (15) (2003) 6050–6055.

[24] D.A. Giannakoudakis, J.A. Arcibar-Orozco, T.J. Bandosz, Effect of GO phase in Zn (OH)2/GO composite on the extent of photocatalytic reactive adsorption of mustard gas surrogate, Appl. Catal. B 183 (2016) 37–46.

[25] V. Singh, et al., Graphene based materials: past, present and future, Prog. Mater. Sci. 56 (8) (2011) 1178–1271.

[26] B. Damasceno, et al., Adsorption capacity comparison between graphene oxide and graphene nanoplatelets for the removal of colored textile dyes from wastewater, Environ. Technol. (2019) 1–22.

[27] Y. Gao, et al., Adsorption and removal of tetracycline antibiotics from aqueous solution by graphene oxide, J. Colloid Interface Sci. 368 (1) (2012) 540–546.

[28] A.V. Talyzin, et al., Temperature dependent structural breathing of hydrated graphite oxide in H2O, Carbon 49 (6) (2011) 1894–1899.

[29] N.A. Travlou, et al., Graphite oxide/chitosan composite for reactive dye removal, Chem. Eng. J. 217 (2013) 256–265.

[30] F. Barroso-Bujans, et al., Permanent adsorption of organic solvents in graphite oxide and its effect on the thermal exfoliation, Carbon 48 (4) (2010) 1079–1087.

[31] M. Seredych, T.J. Bandosz, Removal of ammonia by graphite oxide via its intercalation and reactive adsorption, Carbon (New York, NY) 45 (10) (2007) 2130–2132.

[32] V. Chandra, K.S. Kim, Highly selective adsorption of Hg 2+ by a polypyrrole–reduced graphene oxide composite, Chem. Commun. 47 (13) (2011) 3942–3944.

[33] S.-T. Yang, et al., Folding/aggregation of graphene oxide and its application in Cu2 + removal, J. Colloid Interface Sci. 351 (1) (2010) 122–127.

[34] I. Anastopoulos, et al., Agricultural biomass/waste as adsorbents for toxic metal decontamination of aqueous solutions, J. Mol. Liq. 295 (2019) 111684.

[35] T.A. Johnson, et al., Agricultural and agro-processing wastes as low cost adsorbents for metal removal from wastewater: a review, J. Sci. Ind. Res. 67 (2008) 647–658.

[36] G.A. Haghighat, et al., Aminated graphitic carbon derived from corn stover biomass as adsorbent against antibiotic tetracycline: optimizing the physicochemical parameters, J. Mol. Liq. (2020) 113523.

[37] Z. Shen, et al., Characteristics and mechanisms of nickel adsorption on biochars produced from wheat straw pellets and rice husk, Environ. Sci. Pollut. Res. 24 (14) (2017) 12809–12819.

[38] Y. Guo, et al., Effect of alkali treatment of wheat straw on adsorption of Cu(II) under acidic condition, J. Chem. 2016 (2016) 6326372.

[39] K.M. Mousa, A.H. Taha, Adsorption of Reactive Blue dye onto natural and modified wheat straw, J. Chem. Eng. Process. Technol. 6 (6) (2015) 1.

[40] S. Tursynbolat, et al., Ultrasensitive electrochemical determination of metronidazole based on polydopamine/carboxylic multi-walled carbon nanotubes nanocomposites modified GCE, J. Pharm. Anal. 8 (2) (2018) 124–130.

[41] F.S. Aleanizy, et al., Determination and characterization of metronidazole–kaolin interaction, Saudi Pharm. J. 23 (2) (2015) 167–176.

[42] A. Habibi, et al., Adsorption of metronidazole and spiramycin by an Algerian palygorskite. Effect of modification with tin, Microporous Mesoporous Mater. 268 (2018) 293–302.

[43] S.K. Ghadiri, et al., Adsorption of nitrate onto anionic bio-graphene nanosheet from aqueous solutions: isotherm and kinetic study, J. Mol. Liq. 242 (2017) 1111–1117.

[44] K. Jahangiri, et al., Enhancement adsorption of hexavalent chromium onto modified fly ash from aqueous solution; optimization; isotherm, kinetic and thermodynamic study, J. Dispers. Sci. Technol. 40 (8) (2019) 1147–1158.

[45] S. Chatterjee, et al., Application of Response Surface Methodology for Methylene Blue dye removal from aqueous solution using low cost adsorbent, Chem. Eng. J. 181–182 (2012) 289–299.

[46] M. Davodi, H. Alidadi, A. Ramezani, B.F. Jamali, Z. Bonyadi, Study of the removal efficiency of arsenic from aqueous solutions using Melia azedarach sawdust modified with FeO: isotherm and kinetic studies, Desalin. Water Treat. 137 (2019) 292–299.

[47] N.S. Al-Kadhi, The kinetic and thermodynamic study of the adsorption Lissamine Green B dye by micro-particle of wild plants from aqueous solutions, Egypt. J. Aquat. Res. 45 (3) (2019) 231–238.

[48] J.P. Maity, et al., Removal of fluoride from water through bacterial-surfactin mediated novel hydroxyapatite nanoparticle and its efficiency assessment: Adsorption isotherm, adsorption kinetic and adsorption Thermodynamics, Environ. Nanotechnol. Monit. Manag. 9 (2018) 18–28.

[49] O. Celebi, et al., A radiotracer study of the adsorption behavior of aqueous Ba2+ ions on nanoparticles of zero-valent iron, J. Hazard. Mater. 148 (3) (2007) 761–767.

[50] H. Shahbeig, et al., A new adsorption isotherm model of aqueous solutions on granular activated carbon, World J. Modell. Simul. 9 (4) (2013) 243–254.

[51] M. Samarghandi, et al., Two-Parameter Isotherms of Methyl Orange Sorption by Pinecone Derived Activated Carbon, 2009.

[52] T. Ngulube, et al., Calcined magnesite as an adsorbent for cationic and anionic dyes: characterization, adsorption parameters, isotherms and kinetics study, Heliyon 4 (10) (2018) e00838.

[53] X. Li, et al., Mechanistic insight into the interaction and adsorption of Cr(VI) with zeolitic imidazolate framework-67 microcrystals from aqueous solution, Chem. Eng. J. 274 (2015) 238–246.

[54] D.A. Giannakoudakis, et al., Ultrasound-activated TiO2/GO-based bifunctional photoreactive adsorbents for detoxification of chemical warfare agent surrogate vapors, Chem. Eng. J. 395 (2020) 125099.

[55] J. Zhang, et al., Reduction of graphene oxide via L-ascorbic acid, Chem. Commun. 46 (7) (2010) 1112–1114.

[56] S. Abdolhosseinzadeh, H. Asgharzadeh, H.S. Kim, Fast and fully-scalable synthesis of reduced graphene oxide, Sci. Rep. 5 (2015) 10160.

[57] J. Li, et al., Synthesis of few-layer reduced graphene oxide for lithium-ion battery electrode materials, Ind. Eng. Chem. Res. 53 (34) (2014) 13348–13355.

[58] S. Gurunathan, et al., Reduction of graphene oxide by resveratrol: a novel and simple biological method for the synthesis of an effective anticancer nanotherapeutic molecule, Int. J. Nanomedicine 10 (2015) 2951.

[59] D.R. Dreyer, et al., The chemistry of graphene oxide, Chem. Soc. Rev. 39 (1) (2010) 228–240.

[60] R. Katal, et al., Kinetic, isotherm and thermodynamic study of nitrate adsorption from aqueous solution using modified rice husk, J. Ind. Eng. Chem. 18 (1) (2012) 295–302.

[61] Gaya, U.I., E. Otene, and A.H. Abdullah, Adsorption of aqueous Cd (II) and Pb (II) on activated carbon nanopores prepared by chemical activation of doum palm shell. Springer Plus. 4(1): p. 458.

[62] A. Alazmi, et al., A process to enhance the specific surface area and capacitance of hydrothermally reduced graphene oxide, Nanoscale 8 (41) (2016) 17782–17787.

[63] C. Zhao, et al., A facile route to synthesize transition metal oxide/reduced graphene oxide composites and their lithium storage performance, RSC Adv. 3 (37) (2013) 16597–16603.

[64] M. Du, et al., Synthesis of nitrogen-doped reduced graphene oxide directly from nitrogen-doped graphene oxide as a high-performance lithium ion battery anode, RSC Adv. 4 (80) (2014) 42412–42417.

[65] E.C. Vermisoglou, et al., Effect of hydrothermal reaction time and alkaline conditions on the electrochemical properties of reduced graphene oxide, Appl. Surf. Sci. 358 (2015) 100–109.

[66] H. Dadkhah, M.A. Behnajady, Optimization of photooxidative removal of p-nitrophenol in a spinning disc photoreactor using response surface methodology, Chem. Eng. Commun. 206 (3) (2019) 398–408.

[67] D. Carrales-Alvarado, et al., Removal of the antibiotic metronidazole by adsorption on various carbon materials from aqueous phase, J. Colloid Interface Sci. 436 (2014) 276–285.

[68] J. Rivera-Utrilla, et al., Removal of nitroimidazole antibiotics from aqueous solution by adsorption/bioadsorption on activated carbon, J. Hazard. Mater. 170 (1) (2009) 298–305.

[69] S. Farhadi, et al., Comparison of COD removal from pharmaceutical wastewater by electrocoagulation, photoelectrocoagulation, peroxi-electrocoagulation and peroxi-photoelectrocoagulation processes, J. Hazard. Mater. 219 (2012) 35–42.

[70] E.A. Mehrizi, et al., Isotherms and kinetics of lead and cadmium uptake from the waste leachate by natural absorbent, World Appl. Sci. J. 15 (12) (2011) 1678–1686.

[71] E. Nyankson, et al., Synthesis and kinetic adsorption characteristics of Zeolite/CeO2 nanocomposite, Sci. Afr. 7 (2020) e00257.

[72] Ád.J. Ruíz-Baltazar, et al., Eco-friendly synthesis of Fe3O4 nanoparticles: evaluation of their catalytic activity in methylene blue degradation by kinetic adsorption models, Results Phys. 12 (2019) 989–995.

[73] S. Vasudevan, J. Lakshmi, M. Packiyam, Electrocoagulation studies on removal of cadmium using magnesium electrode, J. Appl. Electrochem. 40 (11) (2010) 2023–2032.

[74] R. Kamaraj, et al., Eco–friendly and easily prepared graphenenanosheets for safe drinking water: removal of chlorophenoxyacetic acid herbicides, ChemistrySelect 2 (1) (2017) 342–355.

[75] N. Jiang, et al., The adsorption mechanisms of organic micropollutants on high-silica zeolites causing S-shaped adsorption isotherms: an experimental and Monte Carlo simulation study, Chem. Eng. J. 389 (2020) 123968.

[76] M.L.F.A. De Castro, et al., Adsorption of Methylene Blue dye and Cu(II) ions on EDTA-modified bentonite: isotherm, kinetic and thermodynamic studies, Sustain. Environ. Res. 28 (5) (2018) 197–205.

[77] S. Vasudevan, J. Lakshmi, The adsorption of phosphate by graphene from aqueous solution, RSC Adv. 2 (12) (2012) 5234–5242.

[78] M.H. Saghi, et al., Fluoride removal from aqueous solution by municipal solid waste compost ash: kinetics, and isotherms studies, Int. J. Environ. Anal. Chem. (2020) 1–13.

[79] N. Aarab, et al., Removal of an emerging pharmaceutical pollutant (metronidazole) using PPY-PANi copolymer: kinetics, equilibrium and DFT identification of adsorption mechanism, Groundw. Sustain. Dev. 11 (2020) 100416.

[80] N. Aarab, et al., Experimental and DFT studies of the removal of pharmaceutical metronidazole from water using polypyrrole, Int. J. Ind. Chem. 10 (3) (2019) 269–279.

[81] A. Amir, Green synthesized Fe3O4/Cellulose nanocomposite suitable adsorbent for metronidazole removal, Polym. Sci. Ser. B (2020).

[82] E. Asgari, A. Sheikhmohammadi, J. Yeganeh, Application of the Fe3O4-chitosan nano-adsorbent for the adsorption of metronidazole from wastewater: optimization, kinetic, thermodynamic and equilibrium studies, Int. J. Biol. Macromol. 164 (2020) 694–706.

[83] D.H. Carrales-Alvarado, et al., Effect of surface area and physical–chemical properties of graphite and graphene-based materials on their adsorption capacity towards metronidazole and trimethoprim antibiotics in aqueous solution, Chem. Eng. J. 402 (2020) 126155.

[84] Alamgir, et al., Effective adsorption of metronidazole antibiotic from water with a stable Zr(IV)-MOFs: insights from DFT, kinetics and thermodynamics studies, J. Environ. Chem. Eng. 8 (1) (2020) 103642.

[85] E.M. Kalhori, et al., Enhancement of the adsorption capacity of the light-weight expanded clay aggregate surface for the metronidazole antibiotic by coating with MgO nanoparticles: studies on the kinetic, isotherm, and effects of environmental parameters, Chemosphere 175 (2017) 8–20.

[86] Malakootiana, M., A. Nasiria, and H. Mahdizadehb, Metronidazole adsorption on CoFe.

[87] S.J. Segovia-Sandoval, et al., Synthesis and characterization of carbon xerogel/graphene hybrids as adsorbents for metronidazole pharmaceutical removal: effect of operating parameters, Sep. Purif. Technol. 237 (2020) 116341.

[88] M.J. Ahmed, S.K. Theydan, Microwave assisted preparation of microporous activated carbon from Siris seed pods for adsorption of metronidazole antibiotic, Chem. Eng. J. 214 (2013) 310–318.

[89] A.K. Rahardjo, et al., Modified Ponorogo bentonite for the removal of ampicillin from wastewater, J. Hazard. Mater. 190 (1) (2011) 1001–1008.

[90] E.K. Putra, et al., Performance of activated carbon and bentonite for adsorption of amoxicillin from wastewater: mechanisms, isotherms and kinetics, Water Res. 43 (9) (2009) 2419–2430.